ARTICLE NO. 80-4100

Stresses in Double-Lap Joints Bonded with a Viscoelastic Adhesive: Part I. Theory and Experimental Corroboration

Joyanto K. Sen*
Hindustan Aeronautics Ltd., Bangalore, India
and
Robert M. Jones†
Southern Methodist University, Dallas, Texas

Stresses and strains are found in a double-lap joint bonded with a linear viscoelastic adhesive. The joint is subjected to a quasi-static load, and the viscoelastic stress analysis is performed with Schapery's Direct Method of transform inversion. The computational tool used with Schapery's Direct Method is the SAAS III finite element program. The joint is modeled such that the variations of stresses and strains through the adhesive thickness can be determined. In Part I, the theory of modeling viscoelastic materials with finite elements is presented. The theoretical results are corroborated with the results of photoelastic and photoviscoelastic analyses of four geometries of double-lap joints. The error in the theoretical result is estimated. The results of a parametric study together with joint design considerations are presented in Part II of this paper.

Introduction

THE use of adhesive as fasteners in structural systems has increased greatly in the last twenty years. In adhesive-bonded joints the load is transferred from one member to the adjoining member over a continuous length of overlap thus avoiding the stress concentrations which occur at several discrete points in bolted joints. Adhesive-bonded joints are increasingly used in critical aircraft and spacecraft components because their strength-to-weight ratios are higher than those of bolted joints. The use of advanced materials, such as fiber-reinforced composites, in aircraft and spacecraft has led to the need for a stress analysis of adhesive-bonded joints free from the limitations of incomplete characterization of adhesives and from the assumptions which greatly oversimplify the actual stress distribution in the joint.

Previous analyses[1-7] are limited to one or several of the following assumptions: 1) the adhesive is isotropic and linearly elastic, 2) the stresses are uniformly distributed through the adhesive thickness, 3) the effect of Poisson's ratio is negligible, 4) the normal stresses in the adhesive parallel to the length of overlap are negligible, and 5) the applied tension load is uniformly distributed in the adherend in line with the free edges of the adhesive. The assumptions in earlier analyses were necessary in order to achieve tractable results within the constraints of the numerical procedures of the day. With modern numerical techniques, such as the finite element method, these constraints can be overcome, and complete stress analysis of adhesive-bonded joints can be performed.

Volkersen[1] analyzed single-lap joints by assuming the adherends do not bend. This assumption results in constant shear stress through the adhesive thickness and in high magnitudes of the shear stresses at the free boundaries of the adhesive layer. Goland and Reissner[2] permit bending of the adherends, but their solution is for two extreme cases of the ratio of the moduli of the adhesive and adherend. For the case most applicable in the aerospace industry, the maximum shear stresses occur at the ends of the overlap. Pahoja[3] analyzes single-lap joints in which the stresses vary across the adhesive thickness. The free boundary conditions for the adhesive and adherends are violated in his solution. In addition, the location and distribution of the applied load is contrary to St. Venant's principle. Renton and Vinson[4] have to date performed the most complete analysis of a single-lap joint, even though the adhesive is elastic and there is no variation of the shear stress through the adhesive thickness. Hahn and Fouser[5] analyze a double-lap joint in which the free boundary conditions are violated and the adhesive properties are not included in the solution. Finite element analyses of adhesive-bonded joints are conducted by Ahluwalia[6] and by Wooley and Carver[7]. Ahluwalia analyzes a double-lap joint, whereas Wooley and Carver analyze a single-lap joint. The usefulness of these finite element analyses is limited because the element sizes are large and the number of elements few. The singular characteristic of the previous analyses is the restriction to elastic behavior of the adhesive.

In the present stress analysis of the double-lap joint subjected to a constant tension load, we will incorporate those features in analysis and material characterization the absence of which limit the usefulness of the previous investigations. These features are 1) the adhesive is linearly viscoelastic, 2) the stresses vary across the adhesive thickness, 3) shear and tear stresses will be coupled, 4) the effect of transverse shear strain and transverse normal stress will be incorporated, and 5) the boundary conditions will be satisfied.

The double-lap adhesive-bonded joint is shown in Fig. 1. The two center adherends are identical components and comprise the main members of a structural system. Two identical splice components, the outer adherends, are bonded on each side of the center adherends to form the joint. The four bonds are identical; thus, the joint is doubly symmetric about the x and y axes. A very small distance, η, separates the center adherends. The *overlap length* is called c for all the bonds. The *overhang* d is sufficiently long such that a uniform stress, σ_a, acts at $y=\eta/2+c+d$. The thickness of the center adherend is $2t_C$, that of the outer adherend t_0, and that of the adhesive t_A. The applied load σ_a is a static load in the y direction. The center and outer adherends are linearly elastic and isotropic. The adhesive used in this study is shown to be

Received May 15, 1979; revision received Feb. 1, 1980.

Index categories: Structural Statics; Materials, Properties of.

*Assistant Chief Design Engineer, Helicopter Design Bureau.
†Professor of Solid Mechanics. Associate Fellow AIAA.

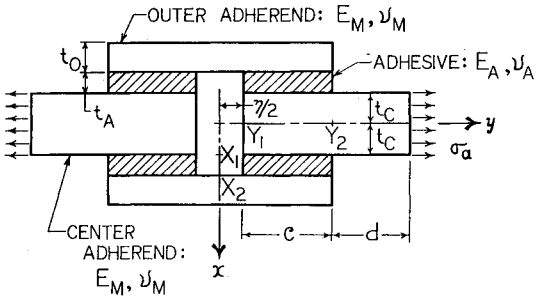

Fig. 1 Double-lap adhesive-bonded joint.

linearly viscoelastic rather than linearly elastic. In addition, the stresses through the adhesive thickness vary.

The joint is analyzed under the condition of plane stress, i.e., the analysis is for the behavior of the joint in the x-y plane, and the width of the joint is such that the stresses perpendicular to the x-y plane are zero. Linear viscoelastic behavior in the finite element analysis is incorporated by use of Schapery's Direct Method in which the Laplace transforms of the applied load and the time-dependent viscoelastic properties are used in a quasi-static analysis.[8] The computational tool is the SAAS III finite element program.[9] The viscoelastic stress distribution in the adhesive and the elastic stress distribution in the adherends are then calculated from the finite element results.

In Part I of this paper, the theories of viscoelastic and photoviscoelastic stress analysis using Schapery's Direct Method of transform inversion[8] are first briefly presented. This presentation is followed by a description of the SAAS III finite element program,[9] the method of application of Schapery's Direct Method in SAAS III, and the finite element model of the double-lap joint. A description of the experimental method of photoviscoelastic analysis is then presented, and, finally, the theoretical results are corroborated with experimental photoviscoelastic and photoelastic results of four geometries of double-lap joints. One joint is analyzed with Schapery's Quasi-Elastic Method[10] in order to determine how good an approximation the solution with this method is to the solution with the Direct Method. The error in the results calculated with Schapery's Direct Method is also estimated.

The results of the parametric study of double-lap joints are presented in Part II of this paper. Moreover, conclusions regarding proper joint design are drawn.

Theoretical Method of Stress Analysis

The basis for the stress analysis of double-lap joints bonded with a viscoelastic adhesive is the theory of linear viscoelastic stress analysis. A viscoelastic problem is generally solved by Alfrey's "correspondence principle."[11] In the correspondence principle, Laplace transforms of the time-dependent boundary conditions and field equations are used to reduce the viscoelastic problem to an "associated elastic problem." Elastic analysis is applied to get the associated elastic solution of the transformed equations. Inversion of the associated elastic solution results in the desired viscoelastic solution.

Two problems arise in the use of the correspondence principle. First, an elastic solution must exist in order to solve the transformed equations. Second, if the mechanical characterization of the viscoelastic material cannot be made in an elementary form, i.e., if the number of terms required to characterize the material is large, then transform inversion of the associated elastic solution is difficult. These problems are alleviated by use of Schapery's Direct Method. Then, an elastic solution is not required because only the numerical values of the transformed material properties are required in order to determine, by whatever means, the associated elastic solution. Furthermore, only the numerical values of the associated elastic solution are necessary to determine the viscoelastic solution. Even more direct than the Direct Method is Schapery's Quasi-Elastic Method.

The computational problems associated with analytical viscoelastic stress analysis are also evident in photoviscoelasticity. In photoviscoelastic stress analysis, the stresses in a viscoelastic model cannot be directly calculated from the measured fringe orders and isoclinics. Schapery's approximate methods can be applied to calculate the stresses in the photoviscoelastic model.

Schapery's approximate methods of transform inversion are first described briefly for both viscoelasticity and photoviscoelasticity. The SAAS III finite element program together with the application of Schapery's Direct Method in SAAS III and the finite element model of the double-lap joint are also described.

Viscoelasticity

In uniaxial tension, an increment of strain, $\Delta\epsilon(\xi)$, applied at time ξ produces an increment of stress, $\Delta\sigma(\xi) = E(t-\xi)\Delta\epsilon(\xi)$, where $E(t)$ is the time-dependent tension modulus of the viscoelastic material being deformed. The incremental stress produced is independent of the values of strain outside the time interval from ξ to $\xi + d\xi$. Thus

$$\Delta\sigma(\xi) = E(t-\xi)\frac{\Delta\epsilon(\xi)}{\Delta\xi}\Delta\xi \tag{1}$$

When $\Delta\xi \to 0$, the stress at time t for a body undisturbed for $t<0$ is

$$\sigma(t) = \int_0^t E(t-\xi)\frac{\partial\epsilon(\xi)}{\partial\xi}d\xi \tag{2}$$

The Laplace transform of Eq. (2), the uniaxial stress-strain relation for a viscoelastic body, is

$$\bar{\sigma}(s) = \bar{E}(s)s\bar{\sigma}(s) \tag{3}$$

where s is the transform parameter. By Schapery's Direct Method, if $\sigma(t)$ has a "small" curvature when plotted against the logarithm of time, then

$$\sigma(t) \approx s\bar{\sigma}(s)\Big|_{s=1/(2t)} \tag{4}$$

for all positive values of s.

In the general case, when a structural component is loaded with a step load P_0, the stress in the x-y plane at time t is

$$\sigma(t) = f[P_0, x, y, E(t), \nu(t)] \tag{5}$$

where $\nu(t)$ is the time-dependent equivalent of Poisson's ratio. The associated elastic solution, $\bar{\sigma}(s)$, is calculated from Eq. (5) with Laplace transformations of the time-dependent functions:

$$\bar{\sigma}(s) = \bar{f}[(P_0/s), x, y, \bar{E}(s), \bar{\nu}(s)] \tag{6}$$

The Laplace transform $\bar{E}(s)$ of the tension modulus is given in terms of the Laplace transform, $\bar{E}_r(s)$, of the tension relaxation modulus[12]

$$\bar{E}(s) = s\bar{E}_r(s) \tag{7}$$

The time-dependent Poisson's Ratio, $\nu(t)$, is similarly related to that determined in a creep test, $\nu_c(t)$:

$$\bar{\nu}(s) = s\bar{\nu}_c(s) \tag{8}$$

Thus, the stress at any time t can be calculated with Eq. (4) for the corresponding values of $\bar{\sigma}(s)$ which are obtained with Eq. (6) for the respective numerical values of $\bar{E}(s)$ and $\bar{\nu}(s)$.

By Schapery's Quasi-Elastic Method, the stress, $\sigma(t_l)$, at time t_l is approximated with Eq. (5) in which the numerical values of $E(t_l)$ and $\nu(t_l)$ are directly used:

$$\sigma(t_l) = f[P_0, x, y, E(t_l), \nu(t_l)] \tag{9}$$

This method is a consequence of the Direct Method because it can be shown that

$$E(t_l) \approx s_l \bar{E}_r(s_l) \quad \nu(t_l) \approx s_l \bar{\nu}(s_l) \tag{10}$$

where $s_l = 1/(2t_l)$.

Photoviscoelasticity

In photoviscoelasticity, the difference of the normal stresses in a body undisturbed for $t<0$ is

$$\sigma_x(t) - \sigma_y(t) = \int_0^t C_\sigma^{-1}(t-\xi) \frac{\partial}{\partial \xi} [N(\xi) \cos 2\theta(\xi)] d\xi \tag{11}$$

where $C_\sigma^{-1}(t)$ is the inverse optical stress coefficient, $N(t)$ the fringe order, and $\theta(t)$ the orientation of the maximum principal light velocity vector to the x axis.

If ψ is the orientation of the maximum principal stress with respect to the x axis, the difference of the maximum stresses is

$$[\sigma_1(t) - \sigma_2(t)] \cos 2\psi = \int_0^t C_\sigma^{-1}(t-\xi) \frac{\partial}{\partial \xi} [N(\xi) \cos 2\theta(\xi)] d\xi \tag{12}$$

If the material is photoviscoelastically simple, i.e., the axes of the principal stresses and strains coincide, then

$$\theta(t) = \psi = \text{constant}$$

and Eq. (12) reduces to

$$\sigma_1(t) - \sigma_2(t) = \int_0^t C_\sigma^{-1}(t-\xi) \frac{\partial N(\xi)}{\partial \xi} d\xi \tag{13}$$

The relative retardation, or the fringe order, is

$$N(t) = \int_0^t C_\sigma(t-\xi) \frac{\partial}{\partial \xi} [\sigma_1(\xi) - \sigma_2(\xi)] d\xi \tag{14}$$

where $C_\sigma(t)$ is the optical stress coefficient. Thus, in the general case

$$N(t) = g[C_\sigma(t), \sigma_1(t) - \sigma_2(t)] \tag{15}$$

By Schapery's Direct Method, if $N(t)$ has a "small" curvature when plotted against the logarithm of time, then

$$N(t) = s\bar{N}(s) \Big|_{s=1/(2t)} \tag{16}$$

if the associated fringe order $\bar{N}(s)$ is known. The associated fringe order can be calculated from

$$\bar{N}(s) = g[\bar{C}_\sigma(s), \bar{\sigma}_1(s) - \bar{\sigma}_2(s)] \tag{17}$$

in which

$$\bar{C}_\sigma(s) = s\bar{C}_{\sigma CRP}(s) \tag{18}$$

where $\bar{C}_{\sigma CRP}(s)$ is the optical stress coefficient in creep and where $\bar{\sigma}_1(s) - \bar{\sigma}_2(s)$ can be calculated from Eq. (6).

By Schapery's Quasi-Elastic Method, with Eq. (9), the fringe order at any time t_l is

$$N(t_l) = g[C(t_l), \sigma_1(t_l) - \sigma_2(t_l)] \tag{19}$$

SAAS III Finite Element Program

The SAAS III program is a very general finite element program for the stress analysis of three-dimensional axisymmetric and two-dimensional plane bodies.[9] The stresses, strains, and displacements are determined through static stress analysis in bodies with orthotropic, temperature-dependent material properties which are different under tension loading than under compression loading. The bodies can be subjected to arbitrary axisymmetric mechanical, thermal, and pore pressure loading. Three features of SAAS III result in considerable efficiency in preparation and computer running time and in accuracy of the results. The first feature is the use of the "mesh generation scheme" to define the coordinates of the nodes of the elements. In the mesh generation scheme, the perimeter of a body is defined with a finite number of line segments. The intermediate points on the perimeter are generated by linear interpolation, and the nodal points interior to the perimeter are determined by satisfying Laplace's equation over a corresponding transformed plane. A second feature is the method of calculating the element strains from the nodal point displacements. The strains are calculated with a linear displacement function which is derived from a least squares fit of the nodal point displacements. A third feature is the accuracy of the results due to reduced discretization errors because a five-point numerical integration scheme is used for calculating the potential energy of the individual elements required in calculating the displacements in the x and y directions for each nodal point.

Application of SAAS III in Schapery's Direct Method

The SAAS III program, as the computational tool in the present application of Schapery's Direct Method for the stress analysis of the double-lap joint, is used as follows:

1) If the viscoelastic solution at time t' is required, calculate the Laplace transform of the adhesive relaxation modulus, $E_r(t)$, for the Laplace parameter $s' = 1/(2t')$. The Laplace transform of the adhesive tension modulus at t' is $\bar{E}(s') = s'\bar{E}_r(s')$.

2) Calculate the Laplace transform of the adhesive Poisson's ratio at time t'. If the Poisson's ratio is constant, the Laplace transform is not taken.

3) The properties of the elastic adherends are constant.

4) The applied load is a step input. The Laplace transform of P_0 at s' is $\bar{P}(s') = P_0/s'$.

5) The solution of the problem with SAAS III leads to the associated elastic solution for stresses, $\bar{\sigma}_{ij}(s')$.

6) The time-dependent viscoelastic response at $t' = 1/(2s')$ is

$$\sigma_{ij}(t') = s'\bar{\sigma}_{ij}(s') \quad \epsilon_{ij}(t') = s'\bar{\epsilon}_{ij}(s') \quad u_i(t') = s'\bar{u}_i(s')$$

7) The photoviscoelastic fringe orders are calculated from the associated elastic solution for the principal stresses,

$$N(t') = s' \bar{C}_\sigma(s') [\bar{\sigma}_1(s') - \bar{\sigma}_2(s')]$$

where $\bar{C}_\sigma(s')$ is the Laplace transform of the optical stress coefficient $C_\sigma(t)$.

If the viscoelastic response at several times is required, a table of values for $s', \bar{E}(s'), \bar{\nu}(s'), \bar{P}(s')$, and $\bar{C}_\sigma(s')$ is constructed for the different times. The associated elastic solution for each time is calculated with SAAS III, and the time-dependent viscoelastic solutions are then calculated with the procedure just outlined.

The Finite Element Model

The double-lap adhesive bonded joint is shown in Fig. 1. One-quarter of the double-lap joint is analyzed because of symmetry about the x and y axes. The finite element model of the joint is designed to yield a good approximation to the stress distribution in the joint. From the results of the previous investigators, we know that the critical sections of the joint are at or near the ends of the overlap where the magnitudes of the stresses and their gradients are high. In contrast, over the middle two-thirds of the overlap, the stress distribution is approximately uniform. Furthermore, the critical regions of the joint are at the adherend-adhesive interfaces. The joint is, therefore, divided into a mesh of elements of different sizes: small elements in regions where the stress gradients are high, and large elements in regions where the stresses are uniform. In addition, the adhesive thickness is divided into a mesh of several elements in order to yield the variation of the stresses through the adhesive thickness.

The finite element model of one-quarter of a joint, identified in Table 1 as joint 1, is shown in Fig. 2. The transformed plane axes, I and J, are parallel to the positive x and y axes. The joint is divided into 22 segments through its thickness and 41 along its length. The line segments in the x-y plane are chosen such that the finite element mesh is finer in the areas of high stress gradients. The adhesive is divided into nine elements through its thickness. The joint has 653 elements and 717 nodal points. The maximum aspect ratio of an element is 10 and occurs in the middle two-thirds of the overlap. The minimum aspect ratio of one occurs in the areas of high stress gradients where the elements are 0.5 mm square. The differences in the geometries of the various joints analyzed are incorporated with as little change in the finite element mesh as possible.

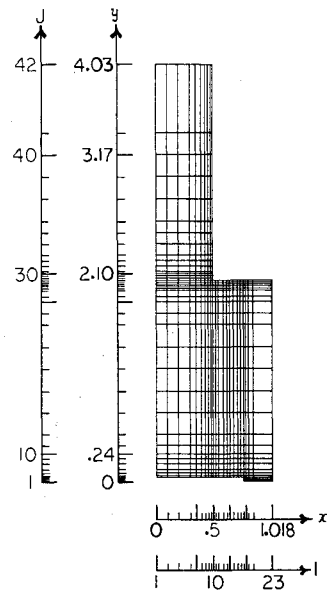

Fig. 2 Finite element model of one-quarter of joint 1.

Experimental Method of Stress Analysis

The experimental analyses for this study are conducted in transmission and scattered-light polariscopes. The analyses performed consist of 1) characterization of the adhesive, 2) photoviscoelastic analyses of three joint geometries, and 3) photoelastic analysis of one three-dimensional joint. The characterization of the adhesive as linearly viscoelastic and as photoviscoelastically simple is described by Sen.[13] The photoviscoelastic analyses of the three joint specimens is conducted in a transmission polariscope because the specimens are two-dimensional. The three-dimensional specimen is analyzed in a scattered-light polariscope.

Table 1 Parameters of the experimental double-lap joints

Parameter	Two-dimensional joints Joint 1	Joint 2	Joint 3	Three-dimensional joint
Adherend material	2014-T3 aluminum	PSM-1 epoxy	2014-T3 aluminum	PLM-4 epoxy
Overlap, c[b]	51.05(2.01)	51.05(2.01)	25.4(1.0)	25.4(1.0)
Overhang, d[b]	127(5.0)	127(5.0)	127(5.0)	63.5(2.5)
Adhesive thickness, t_C[b]	6.81(.268)	6.81(.268)	6.81(.268)	0
Center adherend thickness, t_C[b]	25.4(1.0)	25.4(1.0)	25.4(1.0)	19.05(.75)
Outer adherend thickness, t_0[b]	6.35(.25)	6.35(.25)	6.35(.25)	19.05(.75)
Spacing between center adherends, η	1.52(.06)	1.52(.06)	1.52(.06)	63.5(2.5)
Model width[b]	6.35(.25)	6.35(.25)	6.35(.25)	12.7(.5)
Applied stress, σ_a,MPa, (psi)	1.1(160)	1.1(160)	.27(40)	4.6(667)

[a] The notation is shown in Fig. 1. [b] The dimensions are in millimeters; inch equivalents are given in parentheses.

The tests are conducted with the specimens subjected to a constant load. The two-dimensional specimens are analyzed in the transmission polariscope where the fringe orders and the isoclinics along the edges of the adhesive layer are measured for various times. A maximum of 26 measurements is made along each interface. The measurements are fewer for times shortly after the start of the test because the fringe orders change too rapidly to accomplish 26 measurements.

The test on the three-dimensional specimen, conducted in a scattered-light polariscope, is photoelastic. The time taken to make the measurements in the scattered-light polariscope is longer than in the transmission polariscope, and, therefore, a photoviscoelastic analysis is not attempted. The measurements are made on the center adherend a small distance from the free edge of the adhesive layer, i.e., at $y=\eta/2+c+1.25$. The method of photoelastic analysis is described by Srinath and Frocht.[14]

Materials

The materials for the adhesive-bonded joints used in the experimental stress analysis consist of three materials for the adherends and one material for the adhesive. The adherend materials are 2014-T3 aluminum sheet, and PSM-1 and PLM-4 epoxy materials of Photoelastic, Inc., Malvern, Pa. The three two-dimensional joint specimens are manufactured from 2014-T3 aluminum and PSM-1 epoxy. The three-dimensional specimen is made from PLM-4 epoxy. The adhesive in the two-dimensional specimens is PC-6C epoxy resin, also from Photoelastic. The three-dimensional joint has no adhesive layer.

The mechanical properties of the adherend materials are given in Table 2. These properties are taken directly from the supplier's data sheets. The mechanical properties of the adhesive, as described by Sen[13] are given below, with time t in hours:

Creep compliance

$$D_c(t) = [3.86 - (0.9866e^{-0.01t} + 0.272e^{-0.1t} + 0.801e^{-t})] \times 10^{-9}\,\mathrm{m^2/N}$$

Relaxation modulus

$$E_r(t) = [27.976 + 4.756e^{-0.01t} + 5.665e^{-0.1t} + 9.092e^{-t} + 20.982e^{-10t}] \times 10^{7}\,\mathrm{N/m^2}$$

Constant Poisson's ratio

$$\nu(t) = \nu_A = 0.48$$

Optical stress coefficient

$$C_o(t) = [8.445 - (3.716e^{-0.01t} + 1.745e^{-0.1t} + 0.985e^{-t})] \times 10^{-4}\,\mathrm{fringes - m/N}$$

Inverse optical stress coefficient

$$C^{-1}(t) = [3.553 + 14.742e^{-0.01t} + 8.668e^{-0.1t} + 29.485e^{-t}] \times 10^{2}\,\mathrm{N/fringe\text{-}m}$$

Test Specimens

The double-lap joint specimens are designed to corroborate the results of the finite element analysis of combinations of various materials and geometries. The pertinent parameters of the joints are given in Table 1. The notation in Table 1 is identified in Fig. 1. Joints 1 and 2 have the same geometry but different adherend materials. Joints 1 and 3 have the same materials but different overlap lengths. The adhesive for all three joints is first cast as a single sheet from PC-6C epoxy resin, then cut to size and bonded to the adherends with a small quantity of PC-6C resin. The joints are bonded in molds to prevent misalignment and to reduce shrinkage stresses. The three-dimensional joint is machined from a 25 mm thick sheet cast from PLM-4 epoxy resin. Cab-o-sil is added in a proportion of 0.3 parts per hundred by weight of the resin to enhance light scattering. The joint is of one homogeneous material with zero adhesive thickness. The joint was annealed to remove any residual stresses due to machining.

Table 2 Mechanical properties of adherend materials

Material	Tension modulus, MPa (psi)	Poisson's ratio
2014-T3 aluminum alloy	68,966 (10,000,000)	.33
PSM-1 epoxy	2,345 (340,000)	.38
PLM-4 epoxy	2,931 (425,000)	.36

Correlation of Experimental and Theoretical Results

The theoretical analyses of the double-lap adhesive-bonded joints are made with the finite element method using the SAAS III computer program. The correlation of the theoretical results with the experimental results is designed to show that 1) the finite element model of the joint is accurate, and 2) the incorporation in the SAAS III computer program of the viscoelastic behavior of the adhesive using Schapery's Direct Method is valid.

The experimental results are from the analysis of four joints. In three of the joints, the theoretical results are corroborated by photoviscoelastically measured fringe orders and isoclinics in the adhesive layer. These joints, identified as joints 1,2, and 3 in Table 1, are two-dimensional in geometry. Because the adhesive is photoviscoelastically simple, the fringe orders and the isoclinics are a measure of the directions and magnitudes of the shear stresses. The fourth joint is three-dimensional in geometry. The theoretical magnitudes of the axial normal stress (acting in the direction of the load) in the center adherend are corroborated with photoelastic measurements.

The results measured from the tests on the joints are graphically shown with the predicted theoretical results in Figs. 3-10. The notation used in these figures is identified in Fig. 1. Coordinates X_1 and X_2 are the interfaces of the adhesive layer with the center and outer adherends, respectively. Coordinate Y_1 is the free edge of the adhesive along $y=\eta/2$. Coordinate Y_2 is the other free edge of the adhesive along $y=\eta/2+c$. A variation of the fringe orders with time exists, but there is no variation of the isoclinics. This result is a characteristic of photoviscoelastically simple materials.

The distributions of the measured and predicted fringe orders along the interface $x=X_1$ of the adhesive in joint 1 are shown in Fig. 3. The distributions are for 3.33, 16.67, and 50 h after the start of the test. The times for which the distributions are shown are averages of the times at which the experimental readings are made. The fringe order distribution is nearly uniform over the middle two-thirds of the overlap. As the ends of the overlap are approached, the magnitude of the fringe orders first decreases slightly then rises rapidly to the ends of the overlap. The distribution along the other interface, $x=X_2$ is similar with the decrease near the ends of the overlap more prominent.

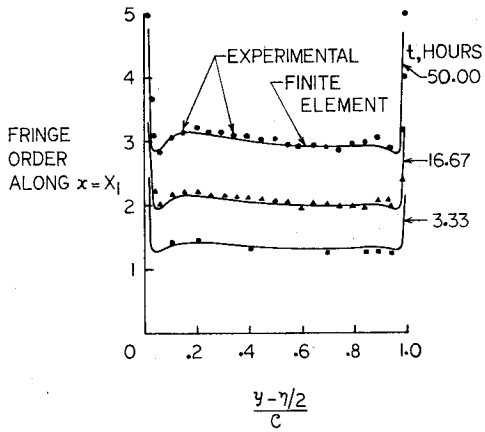

Fig. 3 Experimental and finite element fringe orders in adhesive along x-X_1 in joint 1.

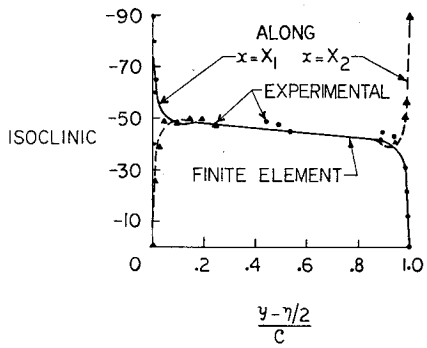

Fig. 4 Experimental and finite element isoclinics in adhesive along the interfaces in joint 1.

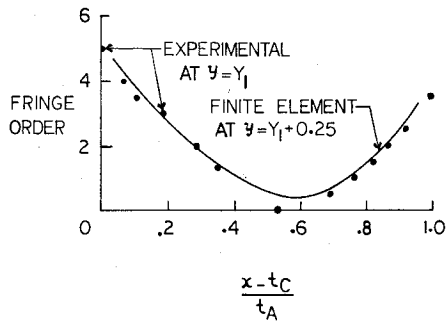

Fig. 5 Experimental and finite element fringe orders in adhesive on and near $y = Y_1$ in joint 1 at time $t = 50$ hours.

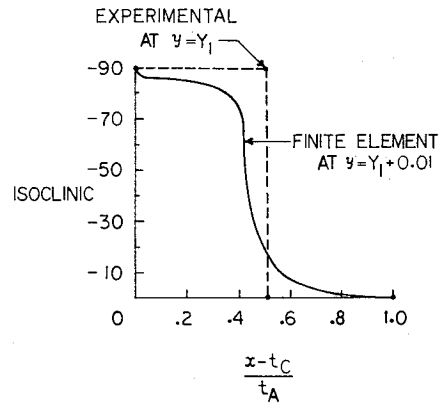

Fig. 6 Experimental and finite element isoclinics in adhesive on and near $y = Y_1$ in joint 1.

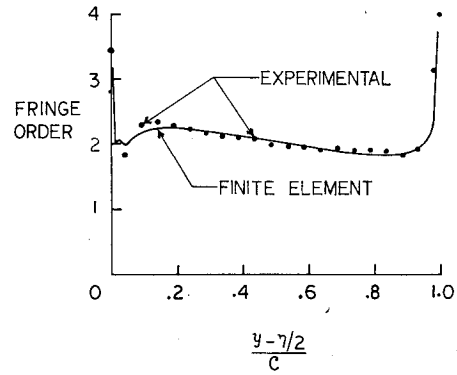

Fig. 7 Experimental and finite element fringe orders in adhesive along $x = X_1$ in joint 2 at time $t = 16.67$ hours.

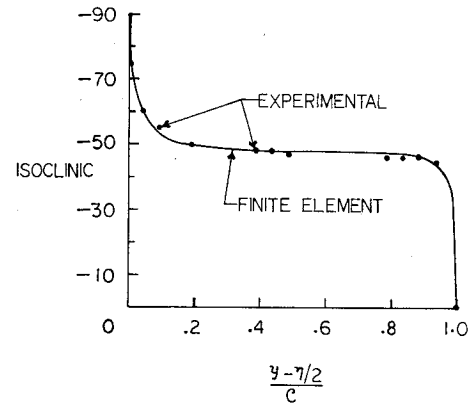

Fig. 8 Experimental and finite element isoclinics in adhesive along $x = X_1$ in joint 2.

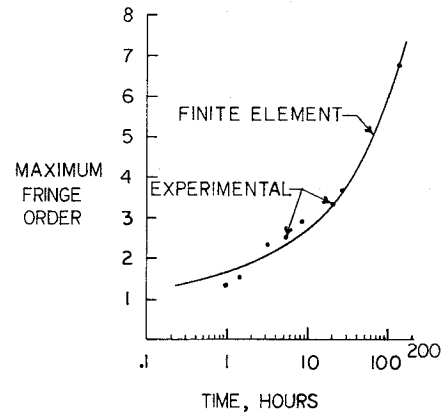

Fig. 9 Experimental and finite element maximum fringe orders at $x = X_1$ in joint 3.

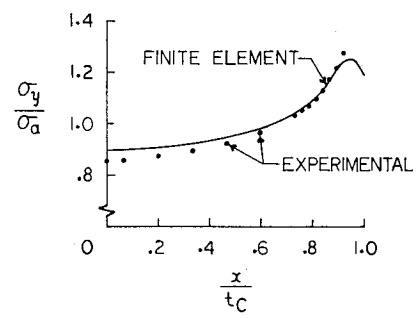

Fig. 10 Experimental and finite element axial normal stress at $y = Y_2 + 1.25$ mm in center adherend of the three-dimensional joint.

Table 3 Adhesive stress concentration factors in the center adherend using the direct and quasi-elastic methods of solution

	Stress concentration factors			
	In shear		In tear	
$(y-\eta/2)/c$	Direct method	Quasi-elastic method	Direct method	Quasi-elastic method
0.005	0.859	0.856	−0.9318	−0.932
0.010	0.934	0.936	−0.5725	−0.572
0.070	0.994	0.992	−0.1433	−0.144
0.180	1.057	1.056	−0.0963	−0.096
0.555	0.988	0.992	0.0025	0.002
0.880	0.988	0.984	0.1293	0.128
0.960	0.920	0.920	0.2413	0.240
0.990	0.945	0.944	0.5033	0.502
0.995	0.992	0.992	0.8675	0.866

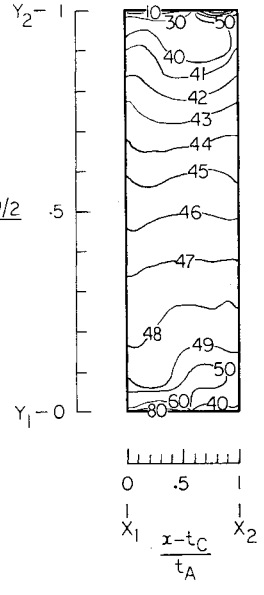

Fig. 11 Isoclinic distribution in adhesive of joint 1.

The isoclinics at the interfaces of joint 1 are shown in Fig. 4. The variation in the magnitudes of the isoclinics over the middle 80% of the overlap is very small (between −41 and −49 deg). At the ends of the overlap (about 10% of the overlap length) the range of the variation is very rapid (from 40 to 50 deg).

The measured fringe orders at the free edge of the adhesive layer ($y=Y_1$) together with the predicted fringe orders 0.25 mm (i.e., one-half the width of the finite element along the free edge) from the edge are shown in Fig. 5. The fringe orders are for joint 1 at 50 h after the start of the test. The fringe order at the center adherend is greater than at the outer adherend. The measured fringe order near the middle of the adhesive layer is zero. The lowest magnitude of the predicted fringe order 0.25 mm from the free edge is not zero. The distributions of the measured and predicted fringe orders at the other free edge, $y=Y_2$, is similar.

The measured and predicted isoclinics at and near the free edge $y=Y_1$ of joint 1 are shown in Fig. 6. Whereas the change in the measured isoclinics from 0 to −90 deg is abrupt (as it would be for a free edge under small deformation), the changes in the predicted isoclinics 0.25 mm from the free edges are gradual. The points at which the isoclinics abruptly change in magnitude are singular, i.e., all isoclinics pass through the points, and the fringe orders are zero. The distribution of the isoclinics along the free edge $y=Y_2$ is similar except that the magnitude is 0 deg at the center adherend and −90 deg at the outer adherend.

The fringe orders along the adhesive interface $x=X_1$ in joint 2 at 16.67 h after the start of the test and the isoclinics at the same interface are shown in Figs. 7 and 8. The distributions for the fringe orders and the isoclinics along the free edge $x=X_2$ are similar with nearly uniform distribution over the middle two-thirds of the overlap and rapidly increasing or decreasing magnitudes as the overlap ends are approached. The variation in the maximum fringe order in the adhesive on the center adherend of joint 3 is shown in Fig. 9. The agreement for times less than 10 h is poor because the rapidly changing fringe orders make measurement of the fractional fringe orders very difficult.

The experimental axial normal stress in the center adherend of the three-dimensional model is shown in Fig. 10. The stress acts in the direction of the applied load at $y=\eta/2+c+1.25$. The theoretical axial normal stress is shown from joint 1. The experimental stresses are calculated at one-half the width of the model, and the agreement between theoretical and experimental stresses is good. The errors in the experimentally determined stresses can be attributed to the shear difference method of photoelasticity.[13] The calculation with the shear difference method is started at the free edge, $x/t_C=1$, and progresses toward $x/t_C=0$. The errors are cumulative and can be seen to occur increasingly in going from $x/t_C=0.6$ to $x/t_C=0$.

Quasi-Elastic Analysis and Error

The double-lap joint, identified as joint 1 in Table 1, is analyzed with the Quasi-Elastic Method using the SAAS III finite element method as the computational tool. The shear and tear stresses in the adhesive interface with the center adherend when analyzed by the Quasi-Elastic and Direct Methods are given in Table 3. The tear stresses are nondimensionalized with respect to the applied stress, σ_a, and the shear stress with respect to the nominal shear stress, $\tau_{nom}=\sigma_a t_C/c$ where the notation is shown in Fig. 1.

The magnitudes of the stress concentration factors, and hence, the stresses, for the two methods of analyses are almost identical. The difference is in the third significant figure. The maximum difference is less than 0.2% and the magnitude of this percentage is not affected by the location and magnitude of the stresses. The stresses in the interface with the outer adherend also exhibit close correspondence when calculated with the two methods.

The error in the theoretical analysis can be estimated by the graphical method suggested by Schapery.[10] The errors in the stresses have been estimated from the errors in the viscoelastic strains because 1) under a constant load, the stresses remain constant, and 2) in the SAAS III finite element program, strains are first calculated from the nodal displacements of the elements before the stresses are determined from the stress-strain relations. In the reference joint, the maximum error in the shear stress is 0.85%, that in the tear stress is 0.77% and that in the axial normal stress is 0.21%.

Concluding Remarks

The experimental and finite element results are in good agreement. Thus, the finite element model chosen to analyze the adhesive-bonded joint is valid, and Schapery's Direct Method is applicable to the finite element analysis of structures with materials which are linearly viscoelastic and photoviscoelastically simple.

The features of the stress distribution in double-lap joints which are evident from the correlation study are 1) the isoclinics (or the directions of the principal stresses) within the adhesive layer are almost the same as those at the interfaces over the middle 80% of the overlap length. This result is graphically shown in Fig. 11. 2) The adhesive is almost in pure shear over the middle 80% of the overlap length. 3) The axial normal stress distribution in the overhang portion of the center adherend is the same for all double-lap joints when the distribution is expressed in nondimensional units.

The Quasi-Elastic Method can be used for stress analysis of joints in order to simplify the numerical procedures. The closeness of the Quasi-Elastic Method results to the Direct Method results suggests that viscoelastic stresses in the joints can be effectively calculated by the Quasi-Elastic Method with instantaneous viscoelastic adhesive properties. The error in the solution using the Direct Method of transform inversion is shown to be negligible and well within the limits of desired engineering accuracy.

A parametric study of the double-lap joint is made in Part II of this paper in order to more fully study and understand the joint. The influences of the various geometric and material parameters are analyzed in order to more effectively design a double-lap joint.

References

[1] Volkersen, O., "Die Nietkraftverteilung in Zugbeanspruchten Nietverbindungen mit konstanten Laschenquerschnitten," *Luftfahrtforschung*, Vol. 15, Jan. 1938, pp. 41-47.

[2] Goland, M. and Reissner, E., "The Stresses in Cemented Joints," *Journal of Applied Mechanics*, Vol. 11, March 1944, pp. A17-A27.

[3] Pahoja, M.H., *Stress Analysis on an Adhesive Lap Joint Subjected to Tension, Shear Force and Bending Moments*, Univ. of Illinois, Urbana-Champaign, Ill., T.&A.M. Rept. 361, Aug. 1972.

[4] Renton, W.J. and Vinson, J.R., *The Analysis and Design of Anisotropic Bonded Joints,* Univ. of Delaware, Newark, Del., Air Force Office of Scientific Research Scientific Rept. AFOSR TR 75-0125, Aug. 1974.

[5] Hahn, K.F. and Fouser, D.F., "Methods of Determining Stress Distributions in Adherends and Adhesives," *Journal of Applied Polymer Science*, Vol. VI, March-April 1962, pp. 145-149.

[6] Ahluwalia, K.S., "Stress Analysis of Double Shear Bonded Joints by the Finite Element Method," M.S. Thesis, Engineering Science Dept., Louisiana State University, Baton Rouge, La., Jan. 1969.

[7] Wooley, G.R. and Carver, D.R., "Stress Concentration Factors for Bonded Lap Joints," *Journal of Aircraft*, Vol. 8, Oct. 1971, pp. 817-820.

[8] Schapery, R.A., "Approximate Methods of Transform Inversion for Viscoelastic Stress Analysis," *Proceedings of the Fourth U.S. National Congress of Applied Mechanics*, Vol. 2, 1962, pp. 1075-1085.

[9] Crose, J.G. and Jones, R.M., *SAAS III, Finite Element Stress Analysis of Anisotropic and Plane Solids with Different Orthotropic, Temperature-Dependent Material Properties in Tension and Compression*, The Aerospace Corp., San Bernardino, Ca., Aerospace Rept. No. TR-0059(S6816-53) – 1, June 1971.

[10] Schapery, R.A., "A Method of Viscoelastic Stress Analysis Using Elastic Solutions," *Journal of the Franklin Institute*, Vol. 279, April 1965, pp. 268-289.

[11] Alfrey, T., "Non-Homogeneous Stresses in Visco-Elastic Media," *Quarterly of Applied Mathematics*, Vol. 2, April 1944, pp. 113-119.

[12] Williams, M.L., "Structural Analysis of Viscoelastic Materials," *AIAA Journal*, Vol. 2, May 1964, pp. 785-808.

[13] Sen, J.K., "The Mechanical and Optical Characterization of a Linear Viscoelastic Material," presented at the Spring Meeting of SESA, Dallas, TX, 15-20 May 1977.

[14] Srinath, L.S. and Frocht, M.M., "The Potentialities of the Method of Scattered Light," *Symposium on Photoelasticity,* edited by M.M. Frocht, The MacMillan Company, New York, 1963.